PCCP

RSC Publishing

PAPER

View Article Online
View Journal | View Issue



Cite this: *Phys. Chem. Chem. Phys.*, 2013, **15**, 2774

# Infrared spectrum of the disilane cation ($Si_2H_6^+$) from Ar-tagging spectroscopy

Marco Savoca, Martin Andreas Robert George, Judith Langer and Otto Dopfer*

Received 25th October 2012,
Accepted 16th December 2012

DOI: 10.1039/c2cp43773b

www.rsc.org/pccp

The infrared spectrum of the disilane cation, $Si_2H_6^+$, in its $^2A_{1g}$ ground state is inferred from photodissociation of cold $Si_2H_6^+$–$Ar_n$ complexes ($n$ = 1, 2). Vibrational analysis is consistent with a $D_{3d}$ symmetric structure of $H_3SiSiH_3^+$ generated by ionization from the bonding $\sigma_{SiSi}$ orbital. Structural, vibrational, and electronic properties of $Si_2H_6^{(+)}$ and $Si_2H_6^+$–$Ar_{1,2}$ are determined at the MP2/aug-cc-pVTZ and B3LYP/aug-cc-pVTZ levels. Ar ligands bind weakly at the $C_3$ axis on opposite sides to $Si_2H_6^+$ with only a minor impact on the $Si_2H_6^+$ properties. The calculations reveal a low-energy $H_2SiHSiH_3^+$ isomer with $C_s$ symmetry and a Si–H–Si bridge, which is only ~15 kJ mol$^{-1}$ above the $D_{3d}$ structure.

## 1. Introduction

Although Si and C are both group IV elements, their bonding characteristics are substantially different. As a result of the much weaker and less directional Si–Si bonds, Si-containing molecules exhibit a larger variety of binding motifs as compared to the corresponding C-bearing species. For example, $Si_xH_y$ molecules often exhibit Si–H–Si bridges,[1–3] which are quite rare for $C_xH_y$. In contrast to the well-characterized $C_xH_y$ molecules, considerably less information is available for the more reactive and less stable $Si_xH_y$ analogues, because precursors for the latter are less readily available. For example, although IR spectra are available for $SiH_y^+$ with $y$ = 3, 5, and 7,[4–6] no vibrational and electronic spectra are available for $Si_xH_y^+$ cations with $x \geq 2$. Characterization of $Si_xH_y$ and their ionic species is not only motivated from fundamental aspects in the theory of chemical bonding but also from understanding of processes in (di)silane plasmas[2,7] and interstellar media.[3,8] In addition, hydrogen passivation of the highly reactive bare silicon clusters and cages has been suggested as a possible route to generate novel stable silicon nanostructures with potential applications in materials science.[9,10] To this end, we set up a program to systematically characterize the geometric and electronic structure of $Si_xH_y$ molecules, their ions, and their clusters by spectroscopy and quantum chemical calculations. Herein we report infrared (IR) spectra of Ar clusters of the disilane cation ($Si_2H_6^+$) obtained by IR photodissociation (IRPD) spectroscopy of mass selected $Si_2H_6^+$–$Ar_n$ clusters, which have been synthesized in a supersonic plasma expansion of $SiH_4$. This tagging approach[11,12] has previously been employed to investigate a variety of fundamental $C_xH_y^+$ ions, including $CH_3^+$,[13–15] $C_2H_2^+$,[16,17] $C_2H_3^+$,[18] $C_3H_3^+$,[19–23] $C_3H_5^+$,[24] $C_6H_{5-7}^+$,[25–34] and $C_{10}H_{16}^+$,[35] as well as $SiOH^+$ cluster ions,[36,37] but seems to be applied for the first time to $Si_xH_y^+$ ions.

Neutral $Si_2H_6$ is a well-characterized molecule. It has a staggered equilibrium structure with $D_{3d}$ symmetry in its $^1A_{1g}$ ground electronic state (Fig. 1). All fundamental vibrational frequencies are accurately known from IR and Raman spectroscopy.[38–41] The geometric parameters of $Si_2H_6$ have been determined by electron diffraction to be $R$ = 2.331(3) Å, $r$ = 1.493(3) Å, and $\theta$ = 110.3(4)°.[42] The threefold barrier for internal rotation *via* the transition state (TS) with $D_{3h}$ symmetry has been determined from high-resolution torsional and tunnelling spectroscopy of IR transitions to be $V_3$ = 407 cm$^{-1}$.[40,41] The 12 vibrational fundamentals of $Si_2H_6$, $\nu_{1-12}$, transform in $D_{3d}$ as $\Gamma_{vib} = 3a_{1g} + a_{1u} + 2a_{2u} + 3e_u + 3e_g$. We follow the notation of vibrational modes given previously in ref. 38 and 39. The fundamentals with $a_{2u}$ ($\nu_{5/6}$) and $e_u$ ($\nu_{7-9}$) symmetry are IR active, whereas those with $a_{1g}$ ($\nu_{1-3}$) and $e_g$ ($\nu_{10-12}$) are Raman active.

In contrast to neutral $Si_2H_6$, surprisingly little spectroscopic and quantum chemical data are available for the corresponding $Si_2H_6^+$ cation and its clusters, probably due to the experimental challenges involved in preparing sufficient number densities of cold (cluster) ions. The limited number of relatively low-level quantum chemical calculations predicts that adiabatic ionization of $Si_2H_6$ occurs from the bonding $\sigma_{Si-Si}$ orbital with $a_{1g}$ symmetry, leading to a $^2A_{1g}$ ground electronic state with staggered configuration ($D_{3d}$).[1,43] As a consequence of ionization to the ionic ground state, the Si–Si bond contracts substantially and the SiSiH bond angle strongly decreases, while the Si–H bond length is less affected. The corresponding values obtained at the MP2/6-31G* level are reported as $\Delta R$ = +0.32 Å, $\Delta\theta$ = −12°, and $\Delta r$ = −0.016 Å, respectively.[1]

*Institut für Optik und Atomare Physik, Technische Universität Berlin, Hardenbergstraße 36, 10623 Berlin, Germany. E-mail: dopfer@physik.tu-berlin.de*

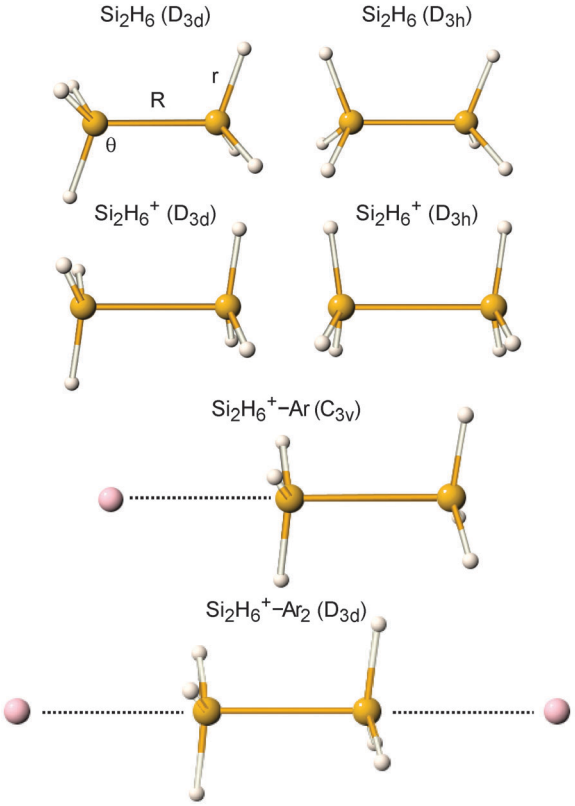


**Fig. 1** Calculated equilibrium structures of $Si_2H_6$ and $Si_2H_6^+$ with $D_{3d}$ and $D_{3h}$ symmetry in their ground electronic states obtained at the B3LYP/aug-cc-pVTZ level. Minimum structures of $Si_2H_6^+$–$Ar_n$ with $n$ = 1 and 2 are given as well. Corresponding geometrical, vibrational, and energetic parameters are listed in Tables 1 and 2.

As a result of the large geometry change upon ionization and the induced long Franck–Condon progressions in the totally symmetric $SiH_3$ umbrella and low-frequency Si–Si stretch modes, the He(I) photoelectron spectrum of $Si_2H_6$ is broad (>1 eV) and essentially unresolved at the achieved spectral resolution ($\sim$200 $cm^{-1}$), largely preventing vibrational characterization of the cation ground state.[44,45] The only vibrationally resolved feature that has been assigned to the symmetric $SiH_3$ umbrella mode is $\nu_2(a_{1g})$ $\sim$ 0.11 eV ($\sim$900 $cm^{-1}$).[45,46] Photoionization mass spectrometry of $Si_2H_6$ yields an adiabatic ionization potential of AIE = 9.74(2) eV, and low appearance energies of $\leq$10.04(2) and $\leq$10.81(2) eV for $H_2$ elimination generating $H_2SiSiH_2^+$ and $HSiSiH_3^+$, respectively.[46]

Here we report IRPD spectra and quantum chemical calculations of $Si_2H_6^+$–$Ar_n$ clusters with $n$ = 1 and 2. The major motivation for this work resulted from the following aspects. (1) The IRPD spectra of cold $Si_2H_6^+$–$Ar_n$ clusters provide the first IR vibrational signatures of the fundamental $Si_2H_6^+$ cation. (2) Neither spectroscopic nor computational data are available for clusters of $Si_2H_6^+$. Hence, this study on $Si_2H_6^+$–$Ar_n$ provides a first impression of the intermolecular interaction of the $Si_2H_6^+$ cation with neutral ligands. (3) *Ab initio* and density functional calculations are performed for $Si_2H_6^+$–$Ar_n$ at the MP2 and B3LYP levels using the aug-cc-pVTZ basis set. Thus, these calculations employ a much higher theoretical level as compared to previous quantum chemical studies. For example, geometry optimization for $Si_2H_6^+$ has only been reported up to the MP2/6-31G* level. The major issues addressed in this work are the effects of ionization and Ar complexation on the geometrical, vibrational, and electronic properties of disilane. We also consider the potential for $SiH_3$ internal rotation because no information appears to exist for the barrier in the ionic ground state. In addition, we explored $Si_2H_6^+$ structures with connectivities other than $H_3SiSiH_3^+$ and report for the first time a low-energy isomer of the disilane cation with a $H_2SiHSiH_3^+$ structure featuring a Si–H–Si bridge.

## 2. Experimental and computational techniques

IRPD spectra of $Si_2H_6^+$–$Ar_n$ with $n$ = 1 and 2 are obtained in a tandem quadrupole mass spectrometer coupled to an electron impact ionization source and an octopole ion trap.[47,48] Weakly-bound $Si_xH_y^+$–$Ar_n$ clusters are generated in a pulsed supersonic plasma expansion by electron impact and chemical ionization of a suitable gas mixture of $SiH_4$ and Ar close to the nozzle orifice and subsequent clustering reactions in the high pressure regime of the expansion. A typical mass spectrum of the ion source obtained for expanding a $SiH_4$/He/Ar mixture with a ratio of 1/20/200 at 5 bar stagnation pressure is shown in Fig. 2. The major cluster series observed are $Ar_n^+$, $Si_xH_y^+$–$Ar_n$, $Si_xH_y^+$–$(SiH_4)_n$, and $Si_xH_y^+$–$(SiH_4)_n$–$Ar_m$. Significant polymerization reactions are observed up to $Si_xH_y^+$ with $x$ = 3. In general, the abundance of $Si_xH_y^+$–$Ar_n$ clusters decreases rapidly with increasing cluster size $n$, consistent with the formation of weakly-bound clusters by sequential addition of individual ligands to the molecular $Si_xH_y^+$ ion. Although the abundance of $Si_2H_6^+$ is at least one order lower compared to the most abundant $Si_xH_y^+$ ions ($SiH_3^+$ and $Si_2H_7^+$), respectable IRPD spectra could be recorded for its weakly-bound $Si_xH_y^+$–$Ar_n$ clusters with $n$ = 1 and 2, illustrating the high sensitivity of the experimental approach. $Si_2H_6^+$–$Ar_n$ ions of interest are mass selected by the first quadrupole and

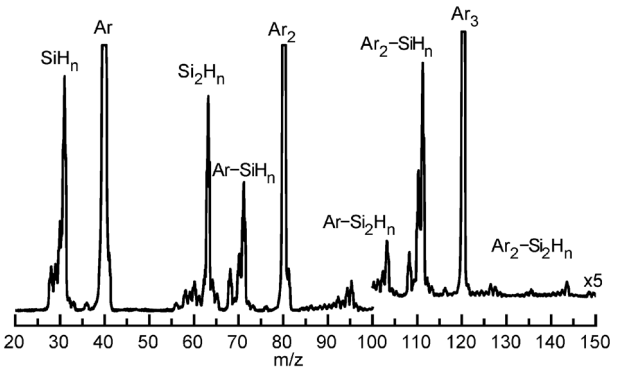


**Fig. 2** Typical mass spectrum of the electron impact cluster ion source for an $SiH_4$/He/Ar expansion (1/20/200) at 5 bar stagnation pressure. Major cluster series observed are $Ar_n^+$, $Si_xH_y^+$–$Ar_n$, $Si_xH_y^+$–$(SiH_4)_n$, and $Si_xH_y^+$–$(SiH_4)_n$–$Ar_m$. Part of the spectrum is vertically expanded by a factor of 5.

irradiated in an adjacent octopole with tuneable IR laser radiation generated by an IR optical parametric oscillator pumped by a Q-switched nanosecond Nd:YAG laser. The IR laser is characterized by a pulse energy of ~0.1–0.5 mJ in the 650–2200 $cm^{-1}$ range, a repetition rate of 10 Hz, and a bandwidth of 1 $cm^{-1}$. Calibration of the IR laser frequency is accomplished by a wavemeter. Resonant vibrational excitation of $Si_2H_6^+$–$Ar_n$ induces evaporation of a single Ar ligand (Ar-tagging), according to:

$$Si_2H_6^+\text{–}Ar_n + h\nu_{IR} \rightarrow Si_2H_6^+\text{–}Ar_m + (n - m)\,Ar \quad (m = n - 1) \tag{1}$$

The resulting $Si_2H_6^+$–$Ar_{n-1}$ fragment ions are selected by the second quadrupole and monitored as a function of the laser frequency to obtain the IR photodissociation spectrum of $Si_2H_6^+$–$Ar_n$. To separate the fragment ions arising from metastable decay and laser-induced dissociation, the ion source is triggered at twice the laser frequency, and signals from alternating triggers are subtracted. Although the IR spectra have been normalized for laser intensity fluctuations, the relative intensities of widely spaced bands are believed to be accurate to within a factor of two, mainly due to the changes in the spatial overlap between the ion and IR laser beams. As the mass spectrum of the ion source is rather complex, collision-induced dissociation (CID) experiments are performed to verify the composition of the mass-selected parent ions. To this end, the octopole is filled with $N_2$ collision gas up to $10^{-5}$ mbar, facilitating single collision conditions with a collision energy of 10 eV in the laboratory frame. The CID spectrum of mass-selected $Si_2H_6^+$–$Ar_2$ in Fig. 3 demonstrates Ar loss as only fragment channels, indicating that the composition of the $m/z$ 142 ion is indeed $102^+$-Ar or $62^+$-$Ar_2$, consistent with the $Si_2H_6^+$–$Ar_2$ parent ion.

$Si_2H_6$, $Si_2H_6^+$, and $Si_2H_6^+$–$Ar_n$ clusters are characterized in their ground electronic states by quantum chemical calculations at the B3LYP and MP2 levels using the cc-pVDZ and aug-cc-pVTZ basis sets,[49] to investigate the effects of ionization and Ar complexation on the geometric, vibrational, and electronic structure as well as the $SiH_3$ internal rotation potential. As the results using the two different basis sets are similar for the monomer species, only the data for the larger aug-cc-pVTZ basis set are reported here. All coordinates are relaxed for the search of stationary points on the potential, and their nature as minimum or transition state (TS) is established by harmonic frequency analysis. Energies are corrected for harmonic zero-point vibrational energy. Harmonic frequencies are scaled by factors of 0.9780 (0.9518) and 0.9942 (0.9742) for B3LYP (MP2) frequencies above and below 1500 $cm^{-1}$, respectively, to optimize the agreement between the calculated and the measured frequencies of $Si_2H_6$. Such a dual scaling factor procedure accounts for the rather different anharmonicity of the Si–H hydride stretch modes and the other vibrations.[50] Application of these scaling factors to the B3LYP (MP2) harmonic frequencies could reproduce the measured frequencies of the fundamentals to better than 13 (18) $cm^{-1}$, with an average deviation of 5 (5) $cm^{-1}$. Spin contamination for the radical cation species is negligible, with values of $<0.006$ and $<10^{-4}$ for $\langle S^2\rangle$ $-0.75$ before and after annihilation, respectively. The charge distribution is calculated using the natural bond orbital (NBO) population analysis.

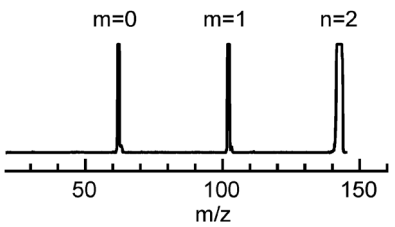


**Fig. 3** CID spectrum obtained by mass-selecting $Si_2H_6^+$–$Ar_2$ ($m/z$ 142) with the first quadrupole and scanning the second quadrupole. The only fragments observed are $Si_2H_6^+$–$Ar_m$ with $m$ = 0 and 1 ($m/z$ 62 and 102) indicating that the composition of the $m/z$ 142 ion is indeed $62^+$-$Ar_2$ or $102^+$-Ar, consistent with $Si_2H_6^+$–$Ar_2$. All peaks are saturated in order to detect possible weak fragment signals.

## 3. Results and discussion

### 3.1 Experimental IR spectra

The IRPD spectra of $Si_2H_6^+$–Ar and $Si_2H_6^+$–$Ar_2$ recorded in the Ar loss channel are shown in Fig. 4. They exhibit only three transitions (**A**–**C**) in the investigated frequency range (650–2230 $cm^{-1}$), consistent with the high symmetry of the $Si_2H_6^+$ ion and the weak perturbation by the Ar ligands. The transitions **A** at 725 and 719 $cm^{-1}$ for $n$ = 1 and 2 are assigned to the antisymmetric linear combination of the umbrella inversion motions, $\nu_6$. The bands **B** at 926 and 925 $cm^{-1}$ for $n$ = 1 and 2 are attributed to the asymmetric $SiH_3$ deformation mode, $\nu_8$. While the assignments of **A** and **B** to fundamentals of $Si_2H_6^+$ are fully supported

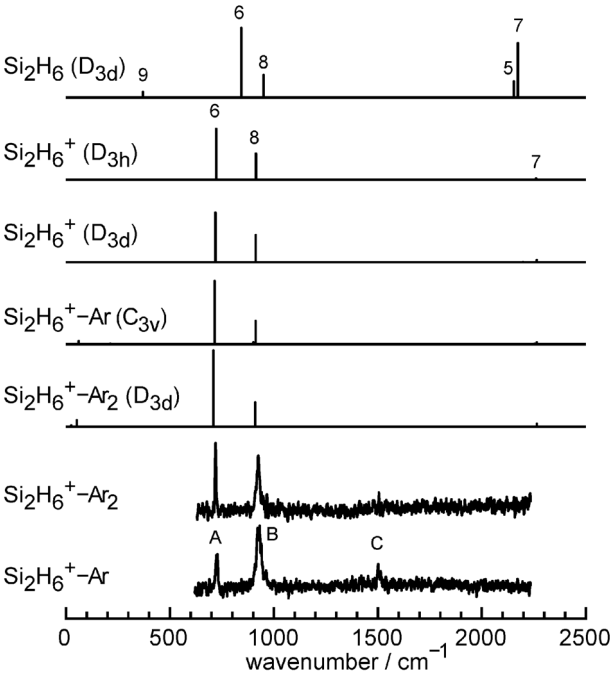


**Fig. 4** Experimental IRPD spectra of $Si_2H_6^+$–Ar and $Si_2H_6^+$–$Ar_2$ compared to linear IR absorption spectra of $Si_2H_6^+$–Ar ($C_{3v}$), $Si_2H_6^+$–$Ar_2$ ($D_{3d}$), $Si_2H_6^+$ ($D_{3d}$, $D_{3h}$), and $Si_2H_6$ ($D_{3d}$) calculated at the B3LYP/aug-cc-pVTZ level (Fig. 1 and Table 2). The calculated spectra are drawn to the same scale.

 

by the calculations presented below, the interpretation of bands C at 1500 and 1505 $cm^{-1}$ for $n = 1$ and 2 is less clear, because $Si_2H_6^+$ does not have any fundamental mode in this frequency range. Currently, the tentative assignment is to the $\nu_6 + \nu_2$ combination band. The $Si_2H_6^+$–$Ar_2$ spectrum could only be obtained in the $Si_2H_6^+$–Ar fragment channel. The fact that no laser-induced dissociation signal was detected in the $Si_2H_6^+$ channel indicates that the IR photon energy of the observed IR resonances is insufficient to evaporate both Ar ligands. The widths of the vibrational transitions (5–25 $cm^{-1}$) result mainly from unresolved rotational fine structure.

Efforts in recording the IR(M)PD spectrum of $Si_2H_6^+$ monitored in the $Si_2H_4^+$ fragment channel failed despite the relatively low reported dissociation energy of $<0.3$ eV ($\sim$2400 $cm^{-1}$). The lack of observation of resonant laser-induced dissociation is ascribed to the single-photon absorption conditions[48,51–53] in connection with the low IR photon energies ($<$2200 $cm^{-1}$) and the high metastable decay background signal observed for $H_2$ elimination of internally hot ions generated in the ion source.

### 3.2 Computational results

The computational results obtained for $Si_2H_6$, $Si_2H_6^+$, and $Si_2H_6^+$–$Ar_n$ relevant for the present work are summarized in Fig. 1, 4, and 5 and Tables 1 and 2, respectively.

In agreement with experiment and previous computations, the global minimum of $Si_2H_6$ in its $^1A_{1g}$ ground electronic state obtained in the present B3LYP and MP2 calculations has a staggered equilibrium structure with $D_{3d}$ symmetry (Fig. 1). The structural parameters of $R_e = 2.35$ Å, $r_e = 1.48$ Å, and $\theta_e = 110^\circ$ agree well with the values derived from electron scattering, $R = 2.331(3)$ Å, $r = 1.493(3)$ Å, and $\theta = 110.3(4)^\circ$.[42] The rotational constants of $A_e = 43\,104$ and $B_e = 5017$ MHz (B3LYP) are also close to the measured values of $A_0 = 43\,208(23)$ and $B_0 = 5120.095(45)$ MHz.[40] Similarly, the scaled fundamental frequencies can reproduce the measured fundamentals well, with a maximum uncertainty of less than 20 $cm^{-1}$. Since the B3LYP values are more accurate, we refer to these frequencies in the text and in Fig. 4, although Table 2 offers also the only slightly less accurate MP2 values. The simulated IR spectrum of $Si_2H_6$ in Fig. 4 shows all five IR active fundamentals with $a_{2u}$ ($\nu_{5/6}$) and $e_u$ ($\nu_{7-9}$) symmetry. These include the two asymmetric Si–H stretch modes $\nu_{5/7}$, the asymmetric umbrella inversion mode $\nu_6$, an asymmetric $SiH_3$ deformation mode $\nu_8$, and an asymmetric $SiH_3$ rocking mode $\nu_9$. The NBO charges of $q_{Si} = 0.6$ e and $q_H = -0.2$ e (MP2) are in line with the higher electronegativity of H. The potential for internal $SiH_3$ rotation of $Si_2H_6$ is shown in Fig. 5. The HSiSiH dihedral angle has been varied in steps of 10°, and for each angle all other coordinates have been relaxed. The threefold barrier occurs at the transition state with eclipsed configuration (0°, Fig. 1, $D_{3h}$) and amounts to $V_3 = 377$ and 336 $cm^{-1}$ at the MP2 and B3LYP levels, respectively, in good agreement with the experimental value of $V_3 = 407$ $cm^{-1}$.[40,41] The geometrical and vibrational parameters of the $D_{3h}$ transition state are quite similar to those of the $D_{3d}$ minimum.

Similar to neutral $Si_2H_6$, the global minimum of $Si_2H_6^+$ in its $^2A_{1g}$ ground electronic state also has a staggered equilibrium structure with $D_{3d}$ symmetry. The adiabatic ionization energies of AIE = 9.49 (9.56) eV calculated at the B3LYP (MP2) level are consistent with the experimental value of AIE = 9.74(2) eV,[46] indicating that the chosen computational approaches describe the electronic structure of $Si_2H_6$ well in both charge states.

**Table 1** Geometrical parameters (in Å and degree), relative energies and binding energies (in $cm^{-1}$), and NBO charge distribution (in e) of the equilibrium structures of $Si_2H_6$, $Si_2H_6^+$, and $Si_2H_6^+$–$Ar_n$ with $n = 1$ and 2 evaluated at the MP2 and B3LYP levels using the aug-cc-pVTZ basis set (Fig. 1)

| | $Si_2H_6$[a] $D_{3d}$ | $Si_2H_6$ $D_{3h}$ (TS) | $Si_2H_6^+$[b] $D_{3d}$ | $Si_2H_6^+$ $D_{3h}$ (TS) | $Si_2H_6^+$–Ar[c] $C_{3v}$ | $Si_2H_6^+$–$Ar_2$ $D_{3d}$ |
|---|---|---|---|---|---|---|
| MP2 | | | | | | |
| $E_{rel}$[d] | 0 | 347 (351) | 0 | 219 (273) | | |
| $D_0$ | | | | | 881 | 815 |
| $R$ | 2.3491 | 2.3601 | 2.7193 | 2.7512 | 2.7193 | 2.7168 |
| $r$ | 1.4812 | 1.4806 | 1.4670 | 1.4667 | 1.4660* | 1.4664 |
| | | | | | 1.4673 | |
| $\theta$ | 110.2 | 110.4 | 98.0 | 98.2 | 96.6* | 97.3 |
| | | | | | 98.6 | |
| $R_{Si-Ar}$ | | | | | 2.9931 | 3.0577 |
| $q_{Si}$ | 0.597 | 0.596 | 0.991 | 0.974 | 0.973* | 0.967 |
| | | | | | 0.980 | |
| $q_H$ | −0.199 | −0.199 | −0.158 | −0.157 | −0.165* | −0.168 |
| | | | | | −0.167 | |
| $q_{Ar}$ | | | | | 0.043 | 0.036 |
| B3LYP | | | | | | |
| $E_{rel}$[d] | 0 | 335 (309) | 0 | 232 (227) | | |
| $D_0$ | | | | | 428 | 364 |
| $R$ | 2.3537 | 2.3655 | 2.7426 | 2.7744 | 2.7451 | 2.7584 |
| $r$ | 1.4858 | 1.4855 | 1.4721 | 1.4732 | 1.4715* | 1.4719 |
| | | | | | 1.4731 | |
| $\theta$ | 110.4 | 110.6 | 98.0 | 98.2 | 96.8* | 97.6 |
| | | | | | 98.7 | |
| $R_{Si-Ar}$ | | | | | 3.1204 | 3.2183 |
| $q_{Si}$ | 0.427 | 0.434 | 0.822 | 0.823 | 0.786* | 0.789 |
| | | | | | 0.814 | |
| $q_H$ | −0.142 | −0.145 | −0.107 | −0.107 | −0.110* | −0.110 |
| | | | | | −0.107 | |
| $q_{Ar}$ | | | | | 0.051 | 0.040 |

[a] Experimental values are $R = 2.331(3)$ Å, $r = 1.493(3)$ Å, and $\theta = 110.3(4)^\circ$.[42] [b] MP2/6-31G* values are $R = 2.659$ Å, $r = 1.487$ Å, and $\theta = 110.4^\circ$.[1] [c] Values of the parameters related to the $SiH_3$ moiety binding to Ar are indicated by asterisks. [d] Numbers in parentheses include zero-point energy.

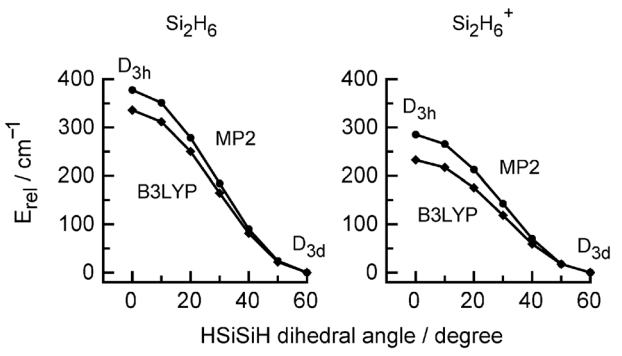


**Fig. 5** Potential for internal $SiH_3$ rotation of $Si_2H_6$ and $Si_2H_6^+$ as a function of the HSiSiH dihedral angle evaluated at the MP2 and B3LYP levels using the aug-cc-pVTZ basis set. The staggered $D_{3d}$ structure (60°) is more stable than the eclipsed $D_{3h}$ geometry (0°) for both charge states.

**Table 2** Experimental and calculated vibrational frequencies (in $cm^{-1}$) of $Si_2H_6$, $Si_2H_6^+$, and $Si_2H_6^+$–$Ar_n$ with $n$ = 1 and 2 evaluated at the MP2 and B3LYP levels using the aug-cc-pVTZ basis set (Fig. 1)[a]

| Mode[b] | Description[c] | $Si_2H_6$[d] $D_{3d}$ | $Si_2H_6$ $D_{3d}$ | $Si_2H_6^+$ $D_{3d}$ | $Si_2H_6^+$ $D_{3h}$ (TS) | $Si_2H_6^+$–Ar $C_{3v}$ | $Si_2H_6^+$–$Ar_2$ $D_{3d}$ |
|---|---|---|---|---|---|---|---|
| $\nu_1(a_{1g})$ | $\sigma_{Si-H}$ | 2163 | 2161 | 2207 | 2209 | 2205 (0.2) | 2208 |
| | | | 2161 | 2201 | 2197 | 2194 (0.5) | 2201 |
| $\nu_2(a_{1g})$ | $\beta_{SiH_3}$ | 920 | 918 | 817 | 826 | 818 (3) | 819 |
| | | | 917 | 787 | 797 | 787 (0.1) | 784 |
| $\nu_3(a_{1g})$ | $\sigma_{Si-Si}$ | 432 | 430 | 233 | 234 | 237 (8) | 243 |
| | | | 419 | 212 | 212 | 214 (5) | 213 |
| $\nu_4(a_{1u})$ | $\tau_{SiH_3}$ | 131.0 | 137 | 116 | *i*113 | 118 | 119 |
| | | | 132 | 94 | *i*93 | 109 | 103 |
| $\nu_5(a_{2u})$ | $\sigma_{Si-H}$ | 2154.3 | 2154 (118) | 2206 (0.1) | 2207 (0.2) | 2210 (0.01) | 2208 (0.3) |
| | | | 2153 (116) | 2198 (1) | 2194 (0.7) | 2201 (0.3) | 2198 (0.05) |
| $\nu_6(a_{2u})$ | $\beta_{SiH_3}$ | 843.5 | 843 (542) | 741 (452) | 742 (470) | 737 (583) | 732 (710) |
| | | | 844 (507) | 718 (360) | 722 (371) | 715 (461) | 709 (554) |
| | | | | | | *725* | *719* |
| $\nu_7(e_u)$ | $\sigma_{Si-H}$ | 2178.6 | 2172 (405) | 2265 (20) | 2267 (20) | 2267 (18) | 2267 (24) |
| | | | 2173 (395) | 2264 (15) | 2260 (15) | 2264 (14) | 2265 (19) |
| $\nu_8(e_u)$ | $\beta_{SiH_3}$ | 939.6 | 953 (184) | 917 (218) | 917 (215) | 915 (187) | 910 (195) |
| | | | 950 (162) | 913 (195) | 914 (191) | 912 (171) | 910 (176) |
| | | | | | | *926* | *925* |
| $\nu_9(e_u)$ | $\gamma_{SiH_3}$ | 379.3 | 362 (46) | 246 (0.5) | 307 (1) | 293 (1) | 356 (1) |
| | | | 370 (41) | 254 (0.1) | 307 (0.2) | 285 (0.2) | 403 (0.02) |
| $\nu_{10}(e_g)$ | $\sigma_{Si-H}$ | 2155? | 2164 | 2260 | 2260 | 2259 (5) | 2260 |
| | | | 2163 | 2257 | 2252 | 2253 (4) | 2257 |
| $\nu_{11}(e_g)$ | $\beta_{SiH_3}$ | 941 | 939 | 906 | 908 | 901 (19) | 899 |
| | | | 936 | 904 | 906 | 901 (14) | 901 |
| $\nu_{12}(e_g)$ | $\gamma_{SiH_3}$ | 628 | 626 | 376 | 348 | 444 (0.04) | 459 |
| | | | 626 | 326 | 307 | 396 (0.02) | 330 (0.5) |
| $\beta$ | | | | | | 57 (2) | 79, 27 (10) |
| | | | | | | 51 (1) | 65, 26 (11) |
| $\sigma$ | | | | | | 74 (28) | 78 (55), 56 |
| | | | | | | 61 (24) | 52 (45), 40 |

[a] IR intensities (in km $mol^{-1}$) of allowed transitions are listed in parentheses. Top (bottom) numbers refer to the MP2 (B3LYP) level. Experimental frequencies are listed in italics. [b] Symmetry given in the $D_{3d}$ point group. [c] Stretch ($\sigma$), rock ($\gamma$), torsion ($\tau$), deformation ($\beta$). [d] From IR and Raman spectra in the gas phase.[38,39,41]

Removal of one electron from the bonding $\sigma_{Si-Si}$ orbital causes the Si–Si bond to drastically elongate by $\Delta R$ = +0.4 Å and the SiSiH bond angle to shrink by $\Delta\theta = -12^\circ$, while the Si–H bonds slightly contract by $\Delta r = -0.014$ Å. These massive structural changes are similar to those predicted at the MP2/6-31G* level[1] and translate directly into the vibrational frequencies and the corresponding IR spectrum. For example, the Si–Si stretch frequency $\nu_3$ is reduced by a factor of 2 from 419 to 212 $cm^{-1}$. The Si–H stretch fundamentals $\nu_{1/5/7/10}$ increase by 40–94 $cm^{-1}$, with an average value of 76 $cm^{-1}$. The $SiH_3$ rocking frequencies $\nu_9$ and $\nu_{12}$ are also reduced by a factor of 1.5 and 2, respectively, and the $SiH_3$ torsional frequency drops by 40%. The symmetric and antisymmetric $SiH_3$ umbrella frequencies $\nu_2$ and $\nu_6$ decrease both by about 15%, while the $SiH_3$ deformation frequencies $\nu_8$ and $\nu_{11}$ decrease merely by $\sim$4%. Thus, with the exception of the Si–H stretch modes, all frequencies are substantially reduced upon removal of the bonding $\sigma_{Si-Si}$ electron, indicating that the force constants for $SiH_3$ rocking, deformation, and torsion as well as Si–Si stretching decrease drastically due to a softer potential in the cation ground state. The potential for internal $SiH_3$ rotation of $Si_2H_6^+$ is similar to that for neutral $Si_2H_6$ (Fig. 5), with the major difference that the barrier at the $D_{3h}$ transition state is lower in the ionic state, $V_3$ = 285 (233) *versus* 377 (336) $cm^{-1}$ at the MP2 (B3LYP) level. Significantly, the barrier in the ionic state is still far too large for tunnelling splittings to be resolved at the current spectral resolution.[41] As the IR spectrum of the $D_{3h}$ transition state is rather similar to that of the $D_{3d}$ global minimum (Fig. 4), the two configurations cannot be distinguished by the current IR spectroscopic experiment. Most frequencies differ by less than 5 $cm^{-1}$, and – as expected – the largest differences are predicted for the two $SiH_3$ rocking frequencies $\nu_9$ and $\nu_{12}$ with 53 and 19 $cm^{-1}$, respectively. The NBO charge distribution of $Si_2H_6$ and $Si_2H_6^+$ detailed in Table 1 suggests that the excess charge arising from ionization from the $\sigma_{Si-Si}$ orbital is indeed fully localized on the Si–Si bond. The resulting charge distribution in the cation ground state at the MP2 (B3LYP) level assigns high positive partial charge to the Si atoms, $q_{Si}$ = +0.99 (+0.82) e, and much smaller negative charges to the H atoms, $q_H = -0.16$ (−0.11) e.

To estimate the influence of Ar complexation on the properties of $Si_2H_6^+$, minima have been searched for on the $Si_2H_6^+$–Ar potential using a variety of starting geometries for energy optimization. The only minimum located at both the MP2 and the B3LYP level is the $C_{3v}$ symmetric structure shown in Fig. 1, in which the Ar ligand binds to one of the $SiH_3$ groups of the $D_{3d}$ conformation of $Si_2H_6^+$ on the $C_3$ symmetry axis (Table 1). In this configuration, the Ar atom can interact optimally with the positively charged Si atom collinear with the partially filled and thus electrophilic $\sigma_{Si-Si}$ orbital. Other starting geometries, in particular those involving H-bonding to

 

the Si–H protons, did not yield minima. This observation is attributed to the high positive partial charge on the Si atoms, which are the main attractors for the Ar ligands. In addition, no minimum was obtained with a $D_{3h}$ symmetric $Si_2H_6^+$ ion core, indicating that the weak interaction with Ar does not invert the torsional potential. At the MP2 level, the intermolecular bond in $Si_2H_6^+$–Ar is characterized by a Si–Ar bond separation of $R_{Si-Ar}$ = 2.99 Å, a dissociation energy of $D_0$ = 881 $cm^{-1}$, and intermolecular bend and stretch frequencies of $\beta$ = 57 and $\sigma$ = 74 $cm^{-1}$, respectively. Ar complexation at this binding site breaks the symmetry between the two $SiH_3$ groups. The Si–Si bond becomes a bit weaker, and there are minor changes in the SiSiH bond angles and Si–H bond lengths of the two non-equivalent $SiH_3$ groups. As expected, the weak interaction with Ar has only little impact on the intramolecular frequencies of $Si_2H_6^+$. Most frequencies change by less than 5 $cm^{-1}$, and – as expected – the largest differences are predicted for the two $SiH_3$ rocking frequencies $\nu_9$ and $\nu_{12}$ with +47 and +68 $cm^{-1}$, respectively. Although symmetry reduction from $D_{3d}$ to $C_{3v}$ upon Ar complexation has the interesting effect that many more modes of $Si_2H_6^+$ become IR active for $Si_2H_6^+$–Ar, namely the $a_{1g}$ ($\nu_{1-3}$) and $e_g$ ($\nu_{10-12}$) modes, their activation is minor in all cases ($I$ < 20 km $mol^{-1}$) due to the weak perturbation and could not be exploited in the present work to detect more vibrational transitions. However, in principle this tagging technique may be used in the future to detect the IR forbidden transitions of $Si_2H_6^+$, such as the interesting Si–Si stretch mode ($\nu_3$) *via* tagging spectroscopy. The attractive part of the intermolecular $Si_2H_6^+$–Ar interaction is mainly based upon charge-induced dipole and dispersion forces. The charge on the Ar ligand is predicted to be less than 0.05 e. As dispersion provides a large contribution to the interaction, the B3LYP level predicts much weaker and longer bonds than the MP2 level (428 *vs.* 881 $cm^{-1}$, 3.12 *vs.* 2.99 Å).

Further complexation with a second Ar ligand on the opposite side of $Si_2H_6^+$–Ar on the $C_3$ axis restores the original $D_{3d}$ symmetry of the monomer cation. The intermolecular bonds in the $n$ = 2 complex are slightly weaker than that for $n$ = 1 ($D_0$ = 815 *vs.* 881 $cm^{-1}$), consistent with the noncooperative three-body induction forces typically observed for solvation of a molecular core ion with neutral nonpolar and inert solvent molecules.[15,22,54–56] These binding energies are compatible with the observed photofragmentation behaviour. Transitions **A** and **B** at around 720 and 925 $cm^{-1}$ are observed only in the single Ar loss channel in both IRPD spectra in Fig. 4.

Finally, we reconsider the spectroscopic assignments of the experimental spectra of $Si_2H_6^+$–$Ar_n$ with $n$ = 1 and 2 given in Section 3.1 in the light of the computational results. Clearly, the transitions **A** at 725 and 719 $cm^{-1}$ for $n$ = 1 and 2 are assigned to the $\nu_6$ fundamental of the $Si_2H_6^+$ moiety in the $Si_2H_6^+$–$Ar_n$ clusters, which are predicted at 715 and 709 $cm^{-1}$, respectively. The B3LYP calculations predict small incremental redshifts for this transition of −3 and −6 $cm^{-1}$, and the latter agrees with the measured shift of −6 $cm^{-1}$. The extrapolated value for the bare $Si_2H_6^+$ ion is thus $\nu_6$ = 728 $cm^{-1}$, and the derived ionization-induced redshift of $\Delta\nu_6$ = −115.5 $cm^{-1}$ matches the predicted value, $\Delta\nu_6$ = −116 $cm^{-1}$. The $\nu_6$ fundamentals in $Si_2H_6^+$–$Ar_n$ with $n$ = 1 and 2 give rise to parallel transitions, which are consistent with the narrow rotational band contours observed (12 and 6 $cm^{-1}$).

The bands **B** at 926 and 925 $cm^{-1}$ for $n$ = 1 and 2 are attributed to the $\nu_8$ fundamental of $Si_2H_6^+$–$Ar_n$, with predicted values of 912 and 910 $cm^{-1}$, respectively. The B3LYP calculations yield incremental redshifts of −1 and −2 $cm^{-1}$, and the latter agrees with the observed shift of −1 $cm^{-1}$. The extrapolated experimental value of $\nu_8$ = 927 $cm^{-1}$ for the isolated $Si_2H_6^+$ ion implies an ionization-induced redshift of $\Delta\nu_8$ = −13 $cm^{-1}$, which is somewhat smaller than the predicted value of $\Delta\nu_8$ = −37 $cm^{-1}$. The $\nu_8$ fundamentals in $Si_2H_6^+$–$Ar_n$ with $n$ = 1 and 2 give rise to perpendicular transitions, and indeed the observed $\nu_8$ rotational band contours are much broader (25 and 20 $cm^{-1}$ for $n$ = 1 and 2) than those of the corresponding parallel $\nu_6$ bands.

The interpretation of bands **C** at 1500 and 1505 $cm^{-1}$ for $n$ = 1 and 2 is less certain, as there is no fundamental of the $Si_2H_6^+$ ion with $D_{3d}$ symmetry in this frequency range. Thus, the first option is an assignment to a combination or overtone band. The only possible candidate involving two vibrational quanta is the symmetry-allowed $\nu_6 + \nu_2$ combination ($a_{2u}$) with predicted frequencies of 1502 and 1493 $cm^{-1}$ for $n$ = 1 and 2 neglecting cross anharmonicities. A second option is an assignment to a $Si_2H_6^+$ isomer with a connectivity different from the $D_{3d}$ structure. It is possible that higher energy isomers of $Si_2H_6^+$ are also formed in the supersonic plasma expansion, which then could be stabilized and cooled in the adiabatic expansion by collisions and subsequent aggregation with Ar. Indeed, we could identify such a low-energy isomer, namely $H_2SiHSiH_3^+$ with $C_s$ symmetry, which is only 15 (16) kJ $mol^{-1}$ less stable than the $D_{3d}$ structure at the MP2 (B3LYP) level. However, as its predicted IR spectrum is quite different from the observed one (Fig. 6), we exclude at the present stage an assignment to higher energy isomers. The calculated $H_2SiHSiH_3^+$ isomer is characterized by a Si–H–Si bridge with a very long Si–Si contact ($R$ = 3.04 Å) and very long Si–H bonds ($r$ = 1.62 and 1.66 Å). Thus, the Si–Si stretch frequency is only 135 $cm^{-1}$ and the asymmetric Si–H–Si

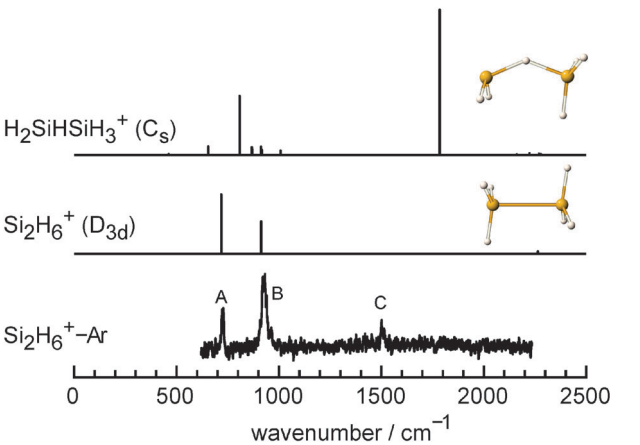


**Fig. 6** Experimental IRPD spectra of $Si_2H_6^+$–Ar compared to linear IR absorption spectra of $H_3SiSiH_3^+$ ($D_{3d}$) and $H_2SiHSiH_3^+$ ($C_s$) isomers calculated at the B3LYP/aug-cc-pVTZ level.

stretch has also an unusually low frequency (1785 $cm^{-1}$) and an enormous IR oscillator strength (882 km $mol^{-1}$). The latter mode is the vibrational IR fingerprint of the Si–H–Si bridge and not observed in the experimental spectra. The third option considered is an assignment to different $X^+$–$Ar_n$ species, which are isobaric to $Si_2H_6^+$–$Ar_n$ with $n$ = 1 and 2. The CID spectra of the ions with $m/z$ 102 and 142 clearly establish that their composition is of the type $62^+$-$Ar_{1/2}$ and $102^+$-Ar (Fig. 3). Possible impurities $X^+$ with $m/z$ 62 are isotopologues of $Si_2H_n^+$ involving $^{29}Si$ or $^{30}Si$ isotopes which occur with natural abundances of 5 and 3%, respectively. Possible candidates for $m/z$ 62 are then $^{28}Si^{29}SiH_5^+$, $^{29}Si_2H_4^+$, $^{30}Si^{28}SiH_4^+$, *etc.* However, we have failed so far to record the IRPD spectra of $^{28}Si_2H_5^+$–$Ar_n$ and $^{28}Si_2H_3^+$–$Ar_n$, and the IRPD spectrum of $^{28}Si_2H_4^+$–Ar also looks different from that of $Si_2H_6^+$–Ar shown in Fig. 4. Other conceivable impurities $X^+$ with $m/z$ 62 involve species with O atoms such as $[SiO_2H_2]^+$ due to the presence of $H_2O$ impurity in the gas inlet system, as evidenced from the weak $(H_2O)_2^+$ peak at $m/z$ 36. However, in the presence of oxygen the $SiH_4$ plasma mass spectrum usually exhibits strong signals for $SiO^+$, $SiOH^+$, and $SiH_3OH_2^+$ at $m/z$ 44, 45, and 49.[36,37] As these ions are completely absent in the mass spectrum in Fig. 2, we also exclude this scenario. In summary, we currently favour the first option with an assignment of bands **C** to $\nu_6 + \nu_2$ of $Si_2H_6^+$–$Ar_n$.

Inspection of Fig. 4 and Table 2 reveals that, although the $Si_2H_6^+$ cation has five IR active transitions, only two of them have high IR oscillator strength ($\nu_6$ and $\nu_8$) and are detected in the present experiment. The three other IR active modes have very low IR oscillator strengths (<20 km $mol^{-1}$) and are also outside the investigated frequency range (650–2200 $cm^{-1}$). Unfortunately, the high IR oscillator strengths of the Si–H stretch fundamentals $\nu_5$ and $\nu_7$ of neutral $Si_2H_6$ (120 and 400 km $mol^{-1}$) are largely quenched upon ionization (1 and 20 km $mol^{-1}$).

The low-resolution photoelectron spectrum exhibits a progression in the symmetric $SiH_3$ umbrella mode measured to be $\nu_2(a_{1g}) \sim 0.11$ eV, which corresponds to $\sim$900 $cm^{-1}$.[45,46] The current calculations predict for this mode a significantly lower frequency of only $\sim$800 $cm^{-1}$ (817 and 787 $cm^{-1}$ at the MP2 and B3LYP level, respectively). As the vibrational assignment is probably correct and the calculations are accurate to better than $\pm$20 $cm^{-1}$, the discrepancy is probably due to the large uncertainty in the photoelectron measurement arising from the low spectral resolution.

## 4. Conclusions

The IR spectrum of the disilane cation, $Si_2H_6^+$, has been inferred from IRPD spectra of cold $Si_2H_6^+$–$Ar_n$ complexes ($n$ = 1 and 2). Vibrational analysis guided by MP2 and B3LYP calculations with the aug-cc-pVTZ basis set is consistent with a $D_{3d}$ symmetric structure of $H_3SiSiH_3^+$ in its $^2A_{1g}$ electronic ground state generated by removal of one electron from the highest occupied bonding $\sigma_{Si-Si}$ orbital. The only intense IR active fundamentals are the $\nu_6$ and $\nu_8$ modes with frequencies of 728 and 927 $cm^{-1}$, respectively. The Ar ligands in $Si_2H_6^+$–Ar and $Si_2H_6^+$–$Ar_2$ bind weakly by induction and dispersion forces at the $C_3$ rotational axis on opposite sides to the $Si_2H_6^+$ core ion and cause only little perturbation of its geometric, vibrational, and electronic structure. The calculations reveal a low-energy $H_2SiHSiH_3^+$ isomer of $Si_2H_6^+$ with $C_s$ symmetry and a Si–H–Si bridge. Although it is predicted to be only $\sim$15 kJ $mol^{-1}$ less stable than the $D_{3d}$ structure, it is not observed in the experimental spectra. Future efforts are directed toward the vibrational and electronic characterization of related $Si_xH_y^+$ ions and their complexes to further investigate their intramolecular chemical bonding characteristics and their interaction with solvent molecules.

## Acknowledgements

This work was supported by TU Berlin and DFG within the research unit FOR 1282 (DO 729/5).

## References

1 L. A. Curtiss, K. Raghavachari, P. W. Deutsch and J. A. Pople, *J. Chem. Phys.*, 1991, **95**, 2433.
2 K. Raghavachari, *J. Chem. Phys.*, 1990, **92**, 452.
3 R. I. Kaiser and Y. Osamura, *Astron. Astrophys.*, 2005, **432**, 559.
4 D. M. Smith, P. M. Martineau and P. B. Davies, *J. Chem. Phys.*, 1992, **96**, 1741.
5 D. W. Boo and Y. T. Lee, *J. Chem. Phys.*, 1995, **103**, 514.
6 Y. B. Cao, J. H. Choi, B. M. Haas, M. S. Johnson and M. Okumura, *J. Phys. Chem.*, 1993, **97**, 5215.
7 W. D. Reents, M. L. Mandich and C. R. C. Wang, *J. Chem. Phys.*, 1992, **97**, 7226.
8 M. C. McCarthy, C. A. Gottlieb and P. Thaddeus, *Mol. Phys.*, 2003, **101**, 697.
9 R. Singh, *J. Phys.: Condens. Matter*, 2008, **20**, 045226.
10 V. Kumar and Y. Kawazoe, *Phys. Rev. Lett.*, 2003, **90**, 055502.
11 M. Okumura, L. I. Yeh, J. D. Myers and Y. T. Lee, *J. Phys. Chem.*, 1990, **94**, 3416.
12 E. J. Bieske and O. Dopfer, *Chem. Rev.*, 2000, **100**, 3963.
13 O. Dopfer, R. V. Olkhov and J. P. Maier, *J. Chem. Phys.*, 2000, **112**, 2176.
14 R. V. Olkhov, S. A. Nizkorodov and O. Dopfer, *J. Chem. Phys.*, 1999, **110**, 9527.
15 R. V. Olkhov, S. A. Nizkorodov and O. Dopfer, *J. Chem. Phys.*, 1998, **108**, 10046.
16 O. Dopfer, R. V. Olkhov, M. Mladenovic and P. Botschwina, *J. Chem. Phys.*, 2004, **121**, 1744.
17 R. A. Relph, J. C. Bopp, J. R. Roscioli and M. A. Johnson, *J. Chem. Phys.*, 2009, **131**, 114305.
18 G. E. Douberly, A. M. Ricks, B. W. Ticknor, W. C. McKee, P. V. R. Schleyer and M. A. Duncan, *J. Phys. Chem. A*, 2008, **112**, 1897.
19 A. M. Ricks, G. E. Douberly, P. V. Schleyer and M. A. Duncan, *J. Chem. Phys.*, 2010, **132**, 051101.
20 P. Botschwina, R. Oswald and O. Dopfer, *Phys. Chem. Chem. Phys.*, 2011, **13**, 14163.
21 D. Roth and O. Dopfer, *Phys. Chem. Chem. Phys.*, 2002, **4**, 4855.

 

22 O. Dopfer, D. Roth and J. P. Maier, *Int. J. Mass Spectrom.*, 2002, **218**, 281.
23 O. Dopfer, D. Roth and J. P. Maier, *J. Am. Chem. Soc.*, 2002, **124**, 494.
24 G. E. Douberly, A. M. Ricks, P. V. R. Schleyer and M. A. Duncan, *J. Chem. Phys.*, 2008, **128**, 4.
25 R. G. Satink, H. Piest, G. von Helden and G. Meijer, *J. Chem. Phys.*, 1999, **111**, 10750.
26 J. M. Bakker, R. G. Satink, G. von Helden and G. Meijer, *Phys. Chem. Chem. Phys.*, 2002, **4**, 24.
27 A. Fujii, E. Fujimaki, T. Ebata and N. Mikami, *J. Chem. Phys.*, 2000, **112**, 6275.
28 G. E. Douberly, A. M. Ricks, P. V. R. Schleyer and M. A. Duncan, *J. Phys. Chem. A*, 2008, **112**, 4869.
29 A. Patzer, S. Chakraborty, N. Solca and O. Dopfer, *Angew. Chem., Int. Ed.*, 2010, **49**, 10145.
30 N. Solcà and O. Dopfer, *Chem.–Eur. J.*, 2003, **9**, 3154.
31 N. Solcà and O. Dopfer, *Angew. Chem., Int. Ed.*, 2002, **41**, 3628.
32 O. Dopfer, R. V. Olkhov and J. P. Maier, *J. Chem. Phys.*, 1999, **111**, 10754.
33 N. Solcà and O. Dopfer, *J. Phys. Chem. A*, 2003, **107**, 4046.
34 N. Solcà and O. Dopfer, *Chem. Phys. Lett.*, 2001, **347**, 59.
35 A. Patzer, M. Schütz, T. Möller and O. Dopfer, *Angew. Chem., Int. Ed.*, 2012, **51**, 4925.
36 R. V. Olkhov and O. Dopfer, *Chem. Phys. Lett.*, 1999, **314**, 215.
37 R. V. Olkhov, S. A. Nizkorodov and O. Dopfer, *Chem. Phys.*, 1998, **239**, 393.
38 G. W. Bethke and M. K. Wilson, *J. Chem. Phys.*, 1957, **26**, 1107.
39 J. R. Durig and J. S. Church, *J. Chem. Phys.*, 1980, **73**, 4784.
40 N. Moazzen-Ahmadi and V. M. Horneman, *J. Chem. Phys.*, 2006, **124**, 194309.
41 F. Lattanzi, C. Di Lauro and V. M. Horneman, *Mol. Phys.*, 2006, **104**, 1795.
42 B. Beagley, J. M. Freeman, A. R. Conrad, B. G. Norton, G. C. Holywell and J. J. Monaghan, *J. Mol. Struct.*, 1972, **11**, 371.
43 J. V. Ortiz and J. W. Mintmire, *J. Am. Chem. Soc.*, 1988, **110**, 4522.
44 H. Bock, W. Ensslin, F. Feher and R. Freund, *J. Am. Chem. Soc*, 1976, **98**, 668.
45 H. Bock, *Angew. Chem., Int. Ed.*, 1989, **28**, 1627.
46 B. Ruscic and J. Berkowitz, *J. Chem. Phys.*, 1991, **95**, 2407.
47 O. Dopfer, *Int. Rev. Phys. Chem.*, 2003, **22**, 437.
48 O. Dopfer, *Z. Phys. Chem.*, 2005, **219**, 125.
49 M. J. Frisch, G. W. Trucks, H. B. Schlegel, G. E. Scuseria, M. A. Robb, J. R. Cheeseman, G. Scalmani, V. Barone, B. Mennucci, G. A. Petersson, H. Nakatsuji, M. Caricato, X. Li, H. P. Hratchian, A. F. Izmaylov, J. Bloino, G. Zheng, J. L. Sonnenberg, M. Hada, M. Ehara, K. Toyota, R. Fukuda, J. Hasegawa, M. Ishida, T. Nakajima, Y. Honda, O. Kitao, H. Nakai, T. Vreven, J. A. Montgomery Jr., J. E. Peralta, F. Ogliaro, M. Bearpark, J. J. Heyd, E. Brothers, K. N. Kudin, V. N. Staroverov, R. Kobayashi, J. Normand, K. Raghavachari, A. Rendell, J. C. Burant, S. S. Iyengar, J. Tomasi, M. Cossi, N. Rega, N. J. Millam, M. Klene, J. E. Knox, J. B. Cross, V. Bakken, C. Adamo, J. Jaramillo, R. Gomperts, R. E. Stratmann, O. Yazyev, A. J. Austin, R. Cammi, C. Pomelli, J. W. Ochterski, R. L. Martin, K. Morokuma, V. G. Zakrzewski, G. A. Voth, P. Salvador, J. J. Dannenberg, S. Dapprich, A. D. Daniels, Ö. Farkas, J. B. Foresman, J. V. Ortiz, J. Cioslowski and D. J. Fox, *GAUSSIAN09, Rev. A.02*, Gaussian, Inc., Wallingford, CT, 2009.
50 M. D. Halls, J. Velkovski and H. B. Schlegel, *Theor. Chem. Acc.*, 2001, **105**, 413.
51 N. Solcà and O. Dopfer, *J. Am. Chem. Soc.*, 2003, **125**, 1421.
52 N. Solcà and O. Dopfer, *Angew. Chem., Int. Ed.*, 2003, **42**, 1537.
53 S. A. Nizkorodov, Y. Spinelli, E. J. Bieske, J. P. Maier and O. Dopfer, *Chem. Phys. Lett.*, 1997, **265**, 303.
54 R. G. Keesee and A. W. Castleman Jr., *J. Phys. Chem. Ref. Data*, 1986, **15**, 1011.
55 O. Dopfer, *Chem. Phys.*, 2002, **283**, 63.
56 O. Dopfer, *J. Phys. Chem. A*, 2000, **104**, 11693.